JOURNAL OF MATERIALS SCIENCE 19 (1984) 4125–4132

Fe–Si–B amorphous alloys with high silicon concentration

A. INOUE, M. KOMURO*, T. MASUMOTO
*The Research Institute for Iron, Steel and Other Metals, and * Graduate School, Tohoku University, Sendai 980, Japan*

Amorphous phase formation with good ductility has been found in Fe–Si–B ternary alloys with high silicon concentration using a melt-spinning technique. The formation range of these amorphous alloys is in the range 0 to 29 at % silicon and 5 to 26 at % boron, being much wider than the previously reported range (0 to 19 at % silicon and 10 to 26 at % boron). The crystallization temperature (T_x) and Vickers hardness (H_v) of the Fe–Si–B amorphous alloys containing more than 19 at % silicon increase significantly with increasing boron content, while the increase in silicon content causes a decrease in T_x and H_v. The T_x and H_v of $Fe_{66}Si_{28}B_6$ alloy with the highest silicon concentration are 740 K and 500 DPN, respectively. The decreases in T_x and H_v with silicon content are interpreted owing to the increase in the contribution of the repulsive interaction between silicon and silicon against the attractive interactions between iron and silicon or boron. Furthermore, the silicon-rich amorphous phase has been found to crystallize by the almost simultaneous precipitation of the two equilibrium compounds of Fe_3Si and Fe_2B, $Fe_2Si_{0.4}B_{0.6}$ or $Fe_{4.9}Si_2B$.

1. Introduction

It is well known that amorphous Fe–Si–B alloys possess good soft ferromagnetic properties [1] combined with high amorphous phase-forming ability [2] and high mechanical strength [3]. Accordingly, they attract increasing interest owing to a high potential for practical use as a soft ferromagnetic material such as a transformer [4]. From such an engineering importance, the amorous phase formation of Fe–Si–B ternary alloys was intensively examined using the roller melt spinning method of single [5, 6] or twin [7] type. According to the results obtained, the formation of the amorphous single phase was limited to the range 0 to 19 at % silicon and 10 to 26 at % boron for the single roller method [5, 6] and 0 to 16 at % silicon and 16 to 23 at % boron for the twin roller method [7], which was located in the boron-rich region compared with silicon concentration. This is because the amorphous phase-forming ability is much higher for Fe–B alloys than for Fe–Si alloys. Such a difference is considered to result from a stronger attractive interaction between iron and boron atoms and a more appropriate atomic size ratio between iron and boron which are favourable for the formation of amorphous phase. However, judging from the equilibrium phase diagram of the Fe–Si binary alloy which indicates the formation of various kinds of iron–silicon compounds and the significant lowering of melting temperature (T_m) by the addition of silicon, an attractive interaction between iron and silicon atoms appears to be rather strong, suggesting that the amorphous phase-forming ability might be relatively high in the vicintiy of about 30 at % silicon. In addition, previous data [5–7] suggest the possibility that an intensive trial to check for the amorphous phase formation of the Fe–Si–B and Fe–Si alloys with high silicon concentration was hardly made even though the amorphous-crystalline phase boundary is represented based on the data of the Fe–Si–B alloys containing less

*Present address: Hitachi Research Laboratory, Hitachi Ltd, Hitachi 317, Japan.

0022–2461/84 $03.00 + .12

than about 18 at% silicon. Therefore, we re-examined the formation range of technologically important Fe–Si–B ternary amorphous alloys and found the amorphous phase formation in a silicon-rich composition range above about 20 at% silicon which is the highest silicon concentration previously reported. The purpose of this paper is to present the composition range for the formation of amorphous Fe–Si–B ternary alloys with high silicon concentration and the hardness, crystallization temperature and crystallization behaviour of the newly found amorphous alloys.

2. Experimental methods

$Fe_{100-x-y}Si_xB_y$ ternary alloy ingots were prepared under an argon atmosphere in an induction furnace from electrolytic iron and pure metalloids (silicon and boron). The melt was sucked up into a quartz tube of about 3 mm i.d. and allowed to solidify. Alloy compositions were expressed by the weighed values in at% because the difference between weighed and chemically analysed compositions was less than 0.05 wt% for silicon and 0.10 wt% for boron. From these master ingots, long ribbons about 1 to 1.5 mm wide and 0.015 to 0.02 mm thick were produced using a single roller type quenching apparatus. The amount of alloy melted in a run was about 2 g and the rotation speed of the steel roller (200 mm diameter) was controlled at about 6000 rpm.

Identification of the as-quenched and annealed phases was made by the X-ray diffractometer using Cu$K\alpha$ radiation in combination with an X-ray monochrometer as well as by transmission electron microscopy. The as-quenched ribbons were classified as being amorphous when the X-ray intensity as a function of diffraction angle showed a typical liquid-like structure. Hardness was measured by a Vickers micro-hardness tester with a 100 g load. Ductility was evaluated by measuring the radius of curvature at fracture in a simple bend test. The crystallization temperature was measured at a heating rate of 10 or 20 K min^{-1} by a differential thermal analyser (DTA) and a differential scanning calorimetry (DSC).

3. Results and discussion

3.1. Formation range of the amorphous phase

Formation of a totally amorphous phase in the Fe–Si–B ternary system was achieved for a much wider range of compositions than that reported so far, as shown in Fig. 1a. The dashed line in Fig. 1 represents the amorphous–crystalline phase boundary taken from [5] and [6] and the formation range of the amorphous phase found in the present work is surrounded by the solid line. As seen in Fig. 1a, a totally amorphous phase was obtained in the range 0 to 29 at% silicon and 5 to 26 at% boron, which is much wider as compared with the previous range [5, 6] of 0 to 19 at% silicon and 10 to 26 at% boron. It is noticed that the present formation range extends to the higher silicon and lower boron concentration side. However, no trace of amorphous phase was found in Fe–Si binary alloys even though the duplex structure consisting of amorphous and crystalline phases is formed in the silicon-rich alloy (Fe–26 at% Si–B) containing a boron content as low as 3 at%, indicating that the dissolution of boron is essential even for the formation of the silicon-rich Fe–Si–B amorphous alloys.

As shown in Fig. 1b, the major region of the Fe–Si–B amorphous phase formation reported so far is located in the phase fields of α(Fe, Si) + Fe_2B, α'(Fe, Si)[Fe_3Si] + Fe_2B, and α' + Fe_2B + $Fe_2Si_{0.4}B_{0.6}$ [7]. This suggests that the formation of the previous amorphous phase is attributed mainly to the high amorhous phase-forming ability of Fe–B binary alloys and the contribution of silicon is supplemental. On the other hand, the boron content in the silicon-rich Fe–Si–B amorphous alloys found in the present work is well below about 13 at% which is a critical minimum content for the formation of the Fe–B binary amorphous alloys, suggesting that an attractive interaction between iron and silicon exerts a significant role on the amorphous phase formation of the silicon-rich alloys. This interpretation is also supported from the equilibrium solidus phase diagram [7] of the Fe–Si–B ternary system represented in Fig. 1b; most of the formation region of the silicon-rich Fe–Si–B amorphous alloys is located in the phase fields of α'(Fe, Si) + Fe_2B, α' + Fe_2B + $Fe_2Si_{0.4}B_{0.6}$, α' + $Fe_{4.9}Si_2B$ + $Fe_2Si_{0.4}B_{0.6}$, and α' + Fe_5Si_3 + $Fe_{4.9}Si_2B$. This is significantly different from the fact [5, 6, 8, 9] that the formation region of the previous amorphous phase extends to the coexisting regions of α(Fe, Si), Fe_2B, α'(Fe, Si) and $Fe_2Si_{0.4}B_{0.6}$. Fig. 1 also suggests that the achievement of a further fast cooling rate might result in the formation of an amorphous phase in the vicinity of about 28 at% silicon even

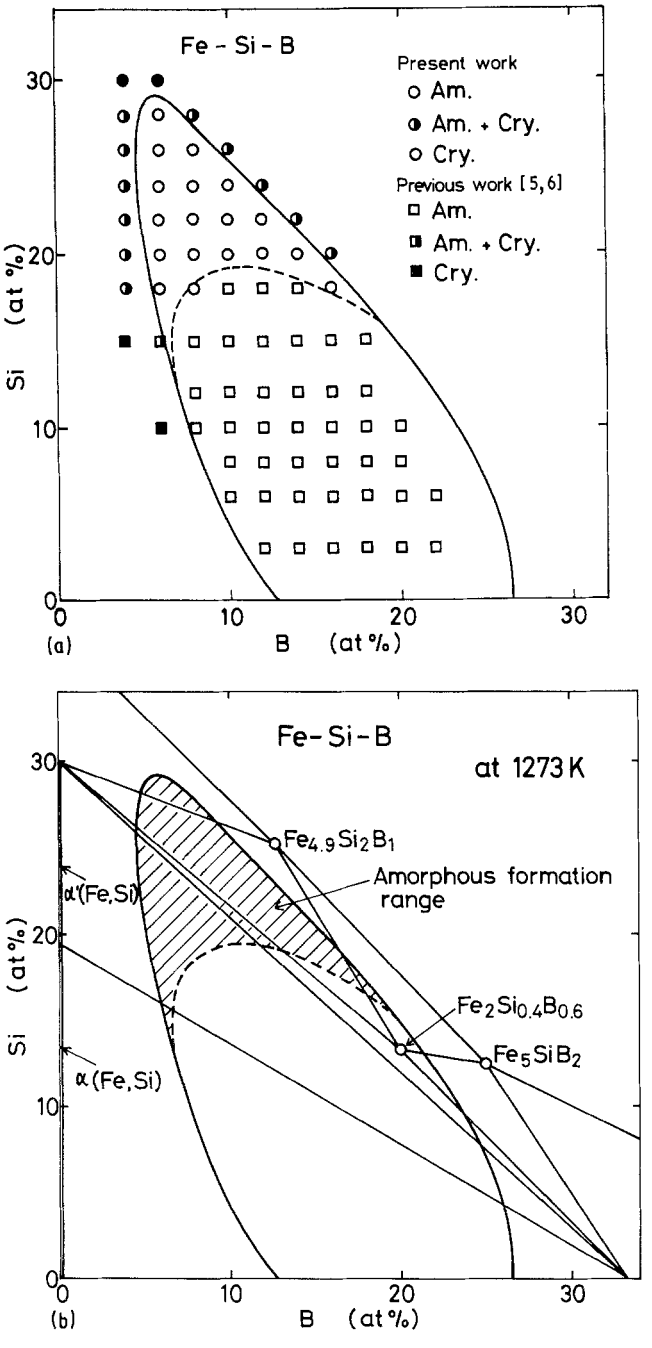

Figure 1 Composition range for the formation of an amorphous phase (a) and equilibrium solidus phase diagram at 1273 K (b) for the Fe–Si–B system. The region surrounded by the dashed line represents the amorphous phase formation range taken from [5] and [6] and the equilibrium phase diagram was taken from [8] and [9].

in Fe–Si binary alloys. The amorphous phase formation of the alloys having a high silicon concentration has also been found in the Fe–Si–P ternary system [10] by the present authors and the detailed results will be presented elsewhere in the near future.

Furthermore, it appears important to point out that all the silicon-rich Fe–Si–B amorphous alloys found in the present work exhibit 180° bend ductility, in spite of the dissolution of the metalloid elements by as much as about 34 at %.

3.2. Crystallization temperature (T_x) and Vickers hardness (H_v)

The compositon dependence of T_x for Fe–Si–B amorphous alloys having a high silicon concentration found in the present work is shown in Fig. 2, where T_x is defined as the onset tempera-

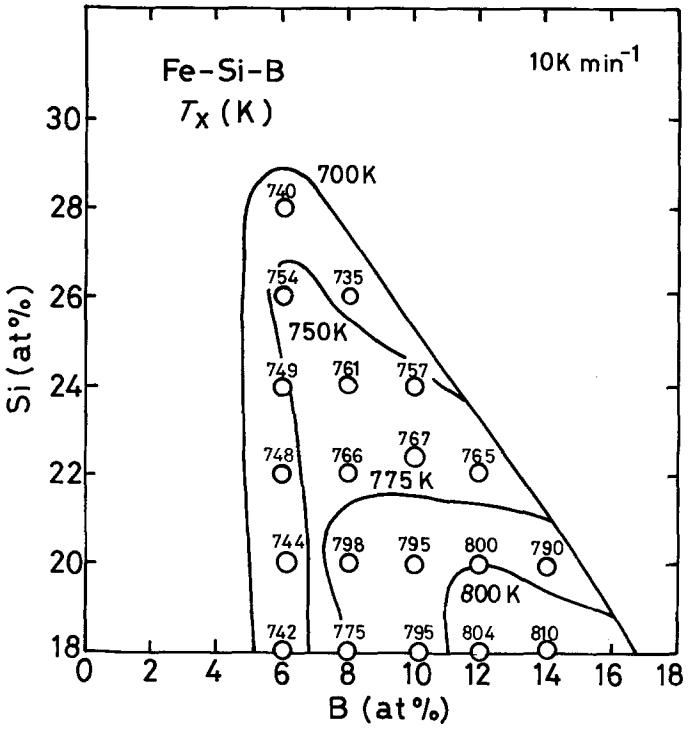

Figure 2 Change in crystallization temperature (T_x) with alloy composition of Fe–Si–B amorphous alloys having high silicon concentrations.

ture of crystallization. The increase in silicon content causes a gradual decrease in T_x and the degree of the decrease becomes smaller with decreasing boron content. On the other hand, an increase in boron content results in a monotonic rise in T_x at 18 at % silicon, and in the range 20 to 24 at % silicon T_x rises once, shows a maximum value at a given boron concentration, and then tends to decrease with further increasing boron content. Thus, the compositional dependence of T_x for the silicon-rich Fe–Si–B amorphous alloys is quite complicated, in good contrast to the simple

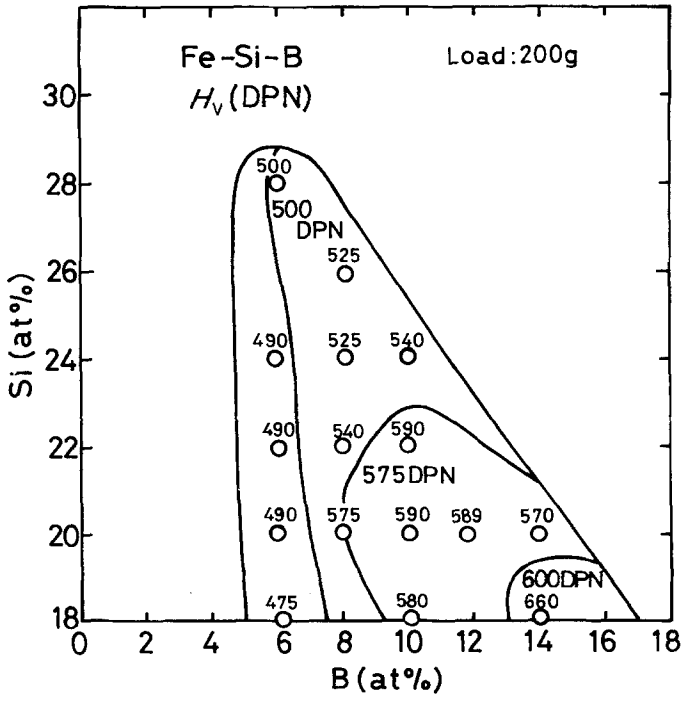

Figure 3 Change in Vickers hardness (H_V) with alloy compositon of Fe–Si–B amorphous alloys having high silicon concentrations.

tendency of the previous Fe–Si–B amorphous alloys where T_x rises monotonically with increasing silicon and boron contents. The most stable alloys against crystallization are located in the vicinity of the alloy composition where the ratio of silicon to boron content is nearly equal to 1 and the total metalloid content is as high as possible. Therefore, it appears that the dissolution of silicon in Fe–Si–B amorphous alloys raises T_x in the range less than about 18 at%, whereas further dissolution of silicon causes a decrease in T_x.

The Vickers hardness (H_v) of the silicon-rich Fe–Si–B amorphous alloys is shown in Fig. 3. Although there is slight scatter, the H_v tends to decrease with the amount of silicon, and the degree of the decrease becomes less with decreasing boron content, similar to the tendency for T_x described above. On the other hand, the dissolution of boron raises the hardness value significantly. As a result, the silicon-rich amorphous alloys with a high hardness are obtained in the vicinity of $Fe_{66}Si_{18}B_{16}$ containing low silicon and high boron contents. Fig. 4 shows the relationship between T_x and H_v for the Fe–Si–B amorphous alloys with high silicon (18 to 28 at%) and low boron (6 to 14 at%) concentrations. There exists a strong correlation between T_x and H_v; the higher the T_x the higher the H_v, similar to the general tendency (e.g. [11]) for a large number of amorphous alloys.

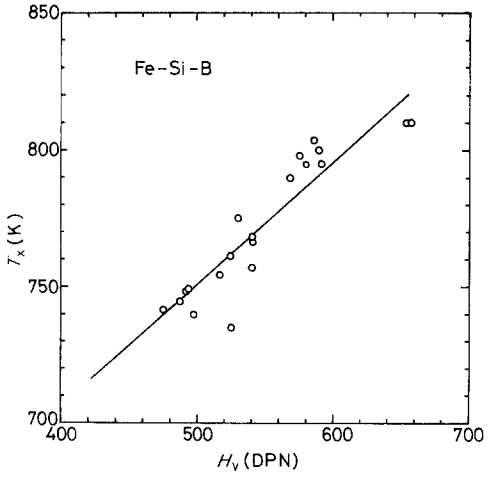

Figure 4 Correlation between crystallization temperature (T_x) and Vickers hardness (H_v) for Fe–Si–B amorphous alloys having high silicon (18 to 28 at%) and low boron (6 to 14 at%) concentrations.

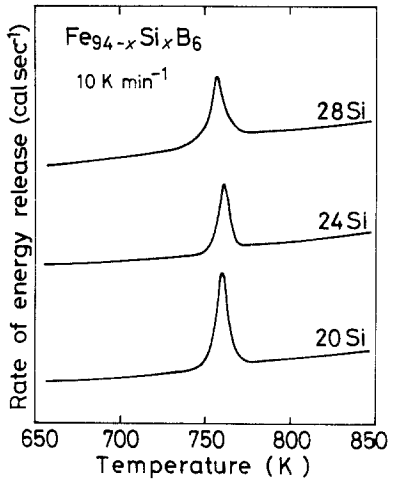

Figure 5 Differential scanning calorimetry curves for $Fe_{74}Si_{20}B_6$, $Fe_{70}Si_{24}B_6$ and $Fe_{66}Si_{28}B_6$ amorphous alloys.

3.3. Crystallization process

Changes in the exothermic peak on the DSC curve were examined for a series of $Fe_{94-x}Si_xB_6$ (x = 18 to 28 at%) amorphous alloys. The general features of the DSC curves for $Fe_{74}Si_{20}B_6$, $Fe_{70}Si_{24}B_6$ and $Fe_{66}Si_{28}B_6$ alloys are shown in Fig. 5. The shape of the DSC curves indicates that the exothermic reaction of these alloys appears to consist of only one peak, even though a slight trace of separation of the peaks is seen for the $Fe_{66}Si_{28}B_6$ alloy. As identified in Figs. 6 to 8, the large exothermic peak results from the simultaneous precipitation of the following two phases; ordered fcc Fe_3Si with a lattice parameter of $\simeq$ 0.565 nm and tetragonal Fe_2B with $a \simeq 0.497$ nm and $c \simeq 0.425$ nm for $Fe_{74}Si_{20}B_6$, Fe_3Si and unidentified compound for $Fe_{70}Si_{24}B_6$ and Fe_3Si and tetragonal $Fe_{4.9}Si_2B$ with $a \simeq 0.882$ nm and $c \simeq 0.434$ nm for $Fe_{66}Si_{28}B_6$. Fig. 9 shows the compositional dependence of the resultant precipitates from the amorpous phase in $Fe_{94-x}Si_xB_6$ alloys. The Fe–Si–B amorpous alloys crystallize to the duplex phases of Fe_3Si and Fe_2B in the range 18 to 23 at% silicon, Fe_3Si and an unidentified compound in the vicintiy of 24 at% silicon and Fe_3Si and $Fe_{4.9}Si_2B$ in the range 25 to 29 at% silicon. These precipitates were compared with the equilibrium solidus phases at a temperature near T_x for Fe–Si–B ternary alloys as shown in Fig. 10. The equilibrium solidus phase near T_x was hypothetically determined from the data of the equilibrium solidus phase diagram at 1273 K of Fe–Si–B ternary alloys and the

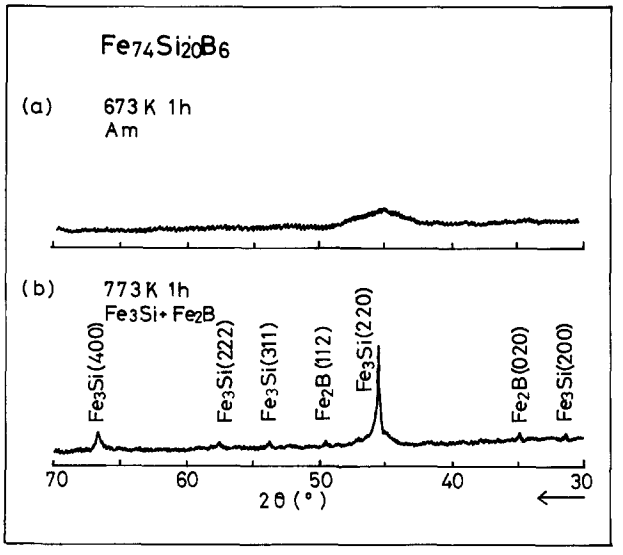

Figure 6 X-ray diffraction patterns as a function of diffraction angle (2θ) for $Fe_{74}Si_{20}B_6$ amorphous alloy annealed for 1 h at (a) 673 K and (b) 773 K.

equilibrium phase diagrams of Fe–Si and Fe–B binary alloys. One can see that each precipitate in the $Fe_{74}Si_{20}B_6$ and $Fe_{66}Si_{28}B_6$ amorphous alloys is completely the same as those in the equilibrium state. From the good agreement between the precipitates from the amorphous and the equilibrium solidus phases, the unknown precipitate in the $Fe_{70}Si_{24}B_6$ amorphous alloys is inferred to be $Fe_2Si_{0.4}B_{0.6}$, even though there is no information available on the crystal structure of the compound.

3.4. Effect of silicon on H_v and T_x

From Figs. 2 to 4, it is clear that the variations of H_v and T_x with composition are very similar for the Fe–Si–B alloys with a high silicon concentration found in the present work, i.e., these values decrease with increasing silicon content and increase with increasing boron content. The change in these values by the addition of 1 at% silicon or boron appears to be much greater for boron than for silicon from the contour of the lines for H_v and T_x shown in Figs. 2 and 3. This

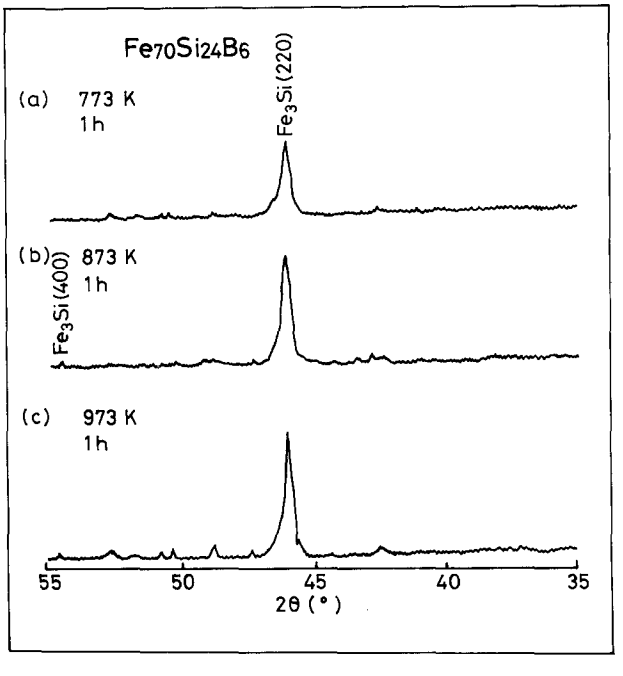

Figure 7 X-ray diffraction patterns as a function of diffraction angle (2θ) for $Fe_{70}Si_{24}B_6$ amorphous alloys annealed for 1 h at (a) 773 K, (b) 873 K and (c) 973 K.

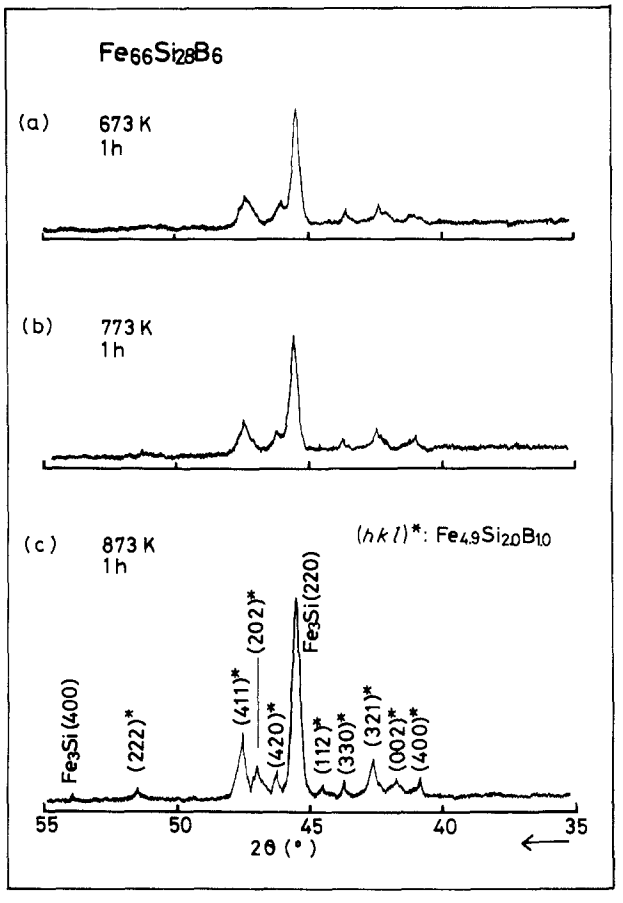

Figure 8 X-ray diffraction patterns as a function of diffraction angle (2θ) for $Fe_{66}Si_{28}B_6$ amorphous alloys annealed for 1 h at (a) 673 K, (b) 773 K and (c) 873 K.

result is dissimilar to the previous results [5, 7] where H_v and T_x for Fe–Si–B amorphous alloys in the range 0 to 19 at% silicon and 10 to 26 at% boron show a larger composition dependence for silicon than for boron. The dissimilar result implies that the bonding force between silicon and the constituent elements increases significantly with increasing silicon content in the range less than about 18 at% silicon, shows a maximum at about 18 at% silicon, and then decreases with further increase in silicon content probably because of the increase in the number of silicon–silicon and silicon–boron bondings with repulsive interaction and the decrease in the number of iron–silicon and iron–boron bondings with attractive interaction. The clearly distinguishable inversion in the contribution of elemental silicon on the increases in T_x and H_v appears to be closely related to the changes in the site which silicon occupies in the amorphous structure. That is, the silicon atom occupies the large polyhedral holes inherent in amorphous structures in the composition range less than about 18 at% silicon and the occupation of the holes by silicon atoms is almost complete at about 18 at% silicon. This situation causes the highest stabilization of the amorphous phase, resulting in the highest T_x and H_v. Further addition of silicon eventually causes

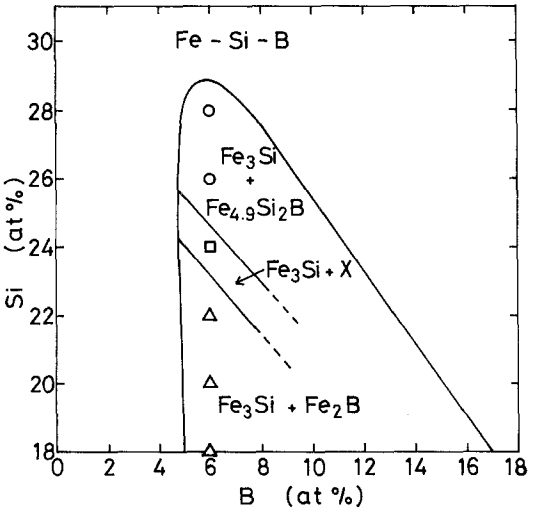

Figure 9 Change in the crystallization-induced precipitates with alloy composition for Fe–Si–B amorphous alloys having high silicon concentrations.

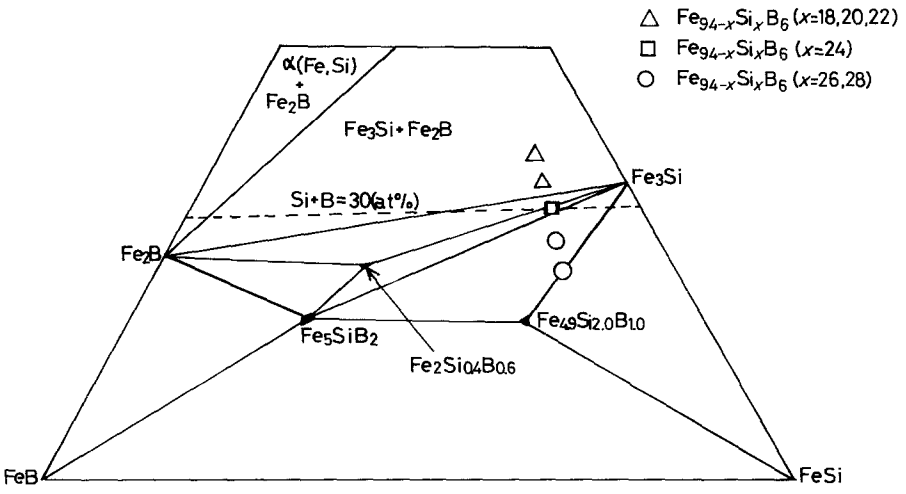

Figure 10 Equilibrium solidus phase diagram near the crystallization temperature for the Fe–Si–B ternary system and the compositions of the alloys where the crystallization process was examined.

the element to occupy energetically unfavourable sites, resulting in the generation of silicon–silicon bonding with repulsive interaction which leads to a lower T_x and H_v of the amorphous phase.

4. Conclusions

Amorphous single phases containing a large amount of silicon have been found in the Fe–Si–B alloy system by a melt quenching techinque. The silicon and boron contents in the amorphous alloys are in the ranges 0 to 29 at % and 5 to 26 at %, respectively, which are much wider than the previously reported ranges (0 to 19 at % silicon and 10 to 26 at % boron). All the amorphous alloys exhibit a good bending ductility in spite of the dissolution of silicon by as much as 29 at %.

The hardness (H_v) and crystallization temperature (T_x) of the Fe–Si–B amorphous alloys with high silicon concentrations ranging from 18 to 28 at %, decrease with increasing silicon content, even though they increase significantly with increasing boron content. For instance, the H_v and T_x values of the $Fe_{66}Si_{28}B_6$ alloy are 500 DPN and 740 K. The decrease in H_v and T_x caused by the dissolution of silicon is interpreted as due to the increase in the number of silicon–silicon and silicon–boron bondings with repulsive interaction and the decrease in the number of iron–silicon and iron–boron bondings with attractive interaction.

The amorphous phase in $Fe_{94-x}Si_xB_6$ ($x \geqslant 18$ at %) alloys crystallizes through the following single process: amorphous → crystal-I + crystal-II. The crystals I and II are the same as the equilibrium solidus phases near T_x in the Fe–Si–B ternary system: ordered f c c Fe_3Si and tetragonal Fe_2B in the range of 18 to 23 at % silicon, Fe_3Si and an unknown precipitate (probably $Fe_2Si_{0.4}B_{0.6}$) in the vicinity of 24 at % silicon, and Fe_3Si and tetragonal $Fe_{4.9}Si_2B$ in the range 25 to 29 at % silicon.

References

1. M. KIKUCHI, H. FUJIMORI, Y. OBI and T. MASUMOTO, *Japan. J. Appl. Phys.* **14** (1975) 1077.
2. M. HAGIWARA, A. INOUE and T. MASUMOTO, *Sci. Rep. Res. Inst. Tohoku Univ.* **A29** (1981) 351.
3. T. MASUMOTO, *ibid.* **A26** (1977) 246.
4. M. MITERA, T. MASUMOTO and N. S. KAZAMA, *J. Appl. Phys.* **50** (1979) 7609.
5. M. NAKA and T. MASUMOTO, *Sci. Rep. Res. Inst. Tohoku Univ.* **A27** (1979) 118.
6. M. HAGIWARA, A. INOUE and T. MASUMOTO, *Met. Trans.* **13** (1982) 373.
7. B. ARONSSON and I. ENGSTROM, *Acta Chem. Scand.* **14** (1960) 1403.
8. A. INOUE, M. KIKUCHI, T. MINEMURA and T. MASUMOTO, *J. Japan Inst. Metals* **42** (1978) 294.
9. *Idem, Sci. Rep. Res. Inst. Tohoku Univ.* **A27** (1979) 127.
10. A. INOUE, M. KOMURO and T. MASUMOTO, unpublished research (1983).
11. H. S. CHEN, *Rep. Prog. Phys.* **43** (1980) 353.

Received 18 January
and accepted 13 March 1984